ARTICLE NO. 80-4063

J80-147

20007
20008
20020

Wave Phenomena in Liquid Jet Breakup in a Supersonic Crossflow

J. A. Schetz,* E. A. Kush Jr.,† and P. B. Joshi‡
Virginia Polytechnic Institute and State University, Blacksburg, Va.

The results of an experimental study of some quantitative features of the wave process that produces jet column fracture are presented. The tests were conducted in a supersonic wind tunnel at Mach 2.4-4.0 at ambient stagnation temperature and stagnation pressures of 2.7-9.5 atm with several injectants at various flow rates. Photographic observations were employed, and data describing the waves on the jet column that lead to breakup including wavelength, amplitude, frequency, and wave speed are presented. The results point toward the "acceleration" mechanism as the mode of wave production.

Nomenclature

a	= wave amplitude
$c \equiv (V_w - V_L)$	= local wave propagation speed
d_j	= injector diameter
M	= Mach number
P_t	= stagnation pressure
q	= dynamic pressure
$\bar{q} \equiv \rho_j V_j^2 / \rho_\infty V_\infty$	= momentum flux ratio
Re/ℓ	= Reynolds number per unit length
V_j	= injection velocity
V_L	= local liquid velocity
V_x	= local axial component of liquid velocity
V_y	= local normal component of liquid velocity
V_w	= local absolute wave velocity
V_∞	= freestream velocity
y	= distance normal to the plate
ρ	= density
λ	= wavelength

Introduction

THE study of a liquid jet injected across a supersonic gas crossflow is of practical importance and theoretical interest. There is a relative scarcity of experimental data pertaining to many details of the process, particularly the primary decomposition mechanism. The immediate stimulus for this study was the experiments of Sherman and Schetz[1] where the presence of large axial waves on the jet, which are the dominant means of jet decomposition by detachment of large masses, was noted. Figure 1 shows a simplified sketch of the major features of the flow. The jet flow is divided into three regions: 1) the cohesive jet body (or deformation zone), 2) the primary and secondary decomposition, or spray formation zone, and 3) the mixing region of fine droplets and air. In the present report, region 1 and the transition from regions 1 and 2 are of principal consideration.

Waves of several types may appear on the jet surface, including small waves due to turbulence and capillary disturbances, but those which are of importance in decomposition are large amplitude waves. They may be due to Rayleigh-Taylor and/or Kelvin-Helmholz instabilities. In the transverse jet problem, the "acceleration" of the Rayleigh-Taylor mode is produced by the aerodynamic drag force due to the crossflow, which causes the jet to curve downstream.

Previous theoretical and experimental work on this and related problems is reviewed in detail in Refs. 2 and 3. In particular, it is shown that recent theories for the present problem are not in accord with experimental observations as to the basic column breakup mechanisms. This experimental study was therefore directed at obtaining a body of quantitative data on the wave breakup process that could be used to develop more adequate theoretical models.

Experimental Apparatus

Facility and Model

The experiments were performed in the VPI & SU 23 × 23 cm supersonic blowdown wind tunnel at ambient stagnation temperature. The stagnation pressure was varied from 2.7 to 6.8 atm at Mach 2.4 and set at 5.4 atm at Mach 3.0 and 9.5 atm at Mach 4.0.

A simple, flat-plate model with dimensions 10 × 13 cm and the jet orifice located 5 cm behind the sharp leading edge was used. The total distance from the plenum chamber under the plate to the surface was 0.3 cm and the straight run of each orifice was 0.16 cm with the port faired into the plenum over the remaining 0.16 cm. Liquid was supplied to the plenum from a pressurized feed system.

Instrumentation

Stop-action pictures were taken with a 0.8 μs duration spark flash and a 15 ns Nanopulser spark unit. Back-lighted pictures with a low light level also gave a shadowgraph effect sufficient to show the jet bow shock shape.

Motion pictures were taken of the jet with a 16 mm movie camera at 36,000 pictures per second. The movies were back-lighted with a 100 W, high-pressure mercury arc light.

A rotating-mirror camera was used to obtain a few frames of pictures at a very high framing rate. The camera runs up to 3000 rps, equivalent to a writing speed of 3.8 mm/μs on the stationary film. The camera was used as a framing device rather than as a streak camera. This was accomplished by using two separate spark flash sources. Two distinct pictures of the jet were recorded on the film, the separation of the pictures being accomplished by the rapid camera rotation. Delay times of 3-15 μs between spark flashes were used. The timing for the spark triggering was accomplished by the electronic system described in Ref. 4.

Received July 2, 1979; revision received Oct. 18, 1979.

Index categories: Jets, Wakes and Viscid-Inviscid Flow Interaction; Multiphase Flows; Wave Motion and Sloshing.

*Professor and Chairman, Dept. of Aerospace and Ocean Engineering. Associate Fellow AIAA.

†Presently at Brookhaven National Laboratory. Member AIAA.

‡Presently at Tetratech, Inc. Member AIAA.

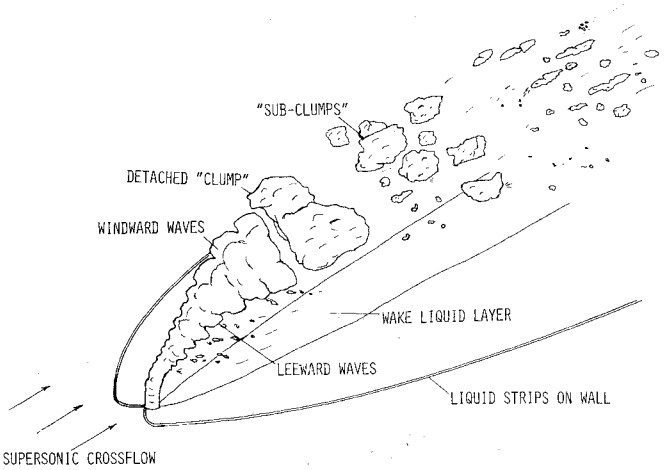

Fig. 1 Isometric sketch of high $\bar{q}$ jet.

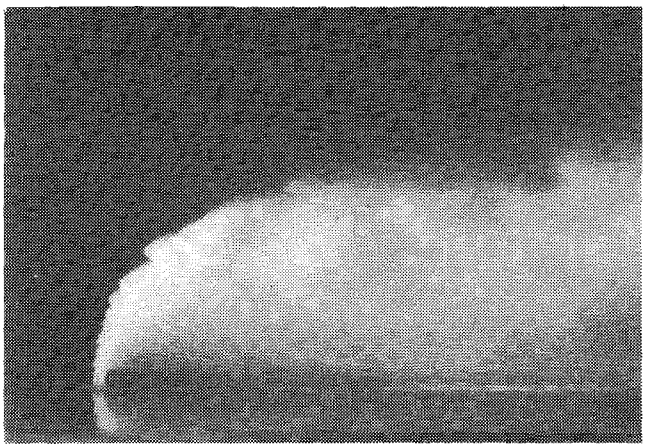

Fig. 2 Typical front-lighted photomicrograph, $\bar{q} = 12.0$.

Test Conditions and Liquid Properties

Many different experimental conditions were studied corresponding to variations in injector size and shape, tunnel stagnation pressure, freestream Mach number, jet liquid, and liquid flow rate. A summary is given in Table 1.

Table 2 is a summary of the pertinent properties of the injectants. Water was used for most tests. The Freons were used in limited amount to investigate vapor pressure effects, and the Freon 12 was heated for a few tests. Carbon disulfide was used because its surface tension and viscosity are similar to those of liquid hydrocarbon fuels. The glycerine-H_2O solution, 30% by volume, was used to study the effects of a large change in liquid viscosity.

Experimental Results

Over 1000 test runs were made. For all jet configurations investigated, high frequency, large amplitude, axially propagating waves were found to be intrinsic to the liquid jet behavior and to be the dominant mechanism in decomposition. This primary breakup consists of gross fracture of the jet column, occurring at a trough between two waves. This could be seen in the back-lighted, photomicrographs.[2,3] The waves extend around the periphery of the jet column. This was observed on front-lighted, spark photographs such as in Fig. 2. This decomposition mode appears similar to the classical Rayleigh jet in quiescent air problem, but the wave nature and cause of fracture are quite different here. The detached "clump" of liquid, usually several wavelengths long, is accelerated downstream and undergoes deformation and decomposition into smaller pieces under the influence of surface tension instability and aerodynamic forces.

The main data to be presented here fall into several categories: 1) wavelength and amplitude measurements from photomicrographs, 2) wave speed measurements with the rotating mirror camera, and 3) jet fracture frequency from the high-speed motion pictures.

Table 1 Experimental variables and wind tunnel conditions for main test program

Variables				
Mach No. = 2.4	Stagnation pressure = 3.4 atm (variations from 2.7 to 6.8 atm)		Stagnation temp. = ambient	
Orifice diameter, cm:		Injectants		
0.079		H_2O, CS_2, glycerine-H_2O		
0.159		H_2O, CS_2, Freon 12 and 21		
0.318		H_2O		
Tunnel freestream conditions:				
M	P_t, atm	V_∞, m/s	q_∞, atm	Re/ℓ, m^{-1}
2.4	3.40	564	0.94	3.3×10^6
2.4	6.80	564	1.88	6.6×10^6

Wavelength and Amplitude Measurements

Waves of a wide range of wavelengths, amplitudes, and shapes were observed, but certain sizes and shapes are usually found in given regions of the jet. We have chosen to nondimensionalize all the wavelengths and amplitudes with the injector diameter even though some of the results do not seem sensitive to that quantity. The "large" waves that lead to breakup include all those bigger than the small ripples seen at the beginning of the jet or as perturbations on the surface of bigger waves, and they have windward wavelengths from about $\lambda/d_j = 0.3$-2.5, with most in the range from $\lambda/d_j = 0.5$ to 1.0. The range of wavelengths is about the same for the two jet diameters tested (0.079 and 0.159 cm), but there are some differences in size and distribution along the jet. The data are all listed in Tables 3 and 4.

The development of the waves on the windward surface may be described by classifying them into three groups. The first group encountered along the jet are short and steep, ranging in wavelength from approximately $\lambda/d_j = 0.3$-0.5. They are regularly spaced, with troughs about equal in size to crests. The amplitude increases at first, then remains nearly constant. The waves first appear at about the same place on

Table 2 Properties of test liquids[a]

Liquid	Specific gravity	Absolute viscosity, kg/ms	Surface tension, N/m	Vapor pressure, atm
H_2O	1.0	9.97×10^{-4}	7.25×10^{-2}	0.02
CS_2	1.27	3.60×10^{-4}	3.25×10^{-2}	0.40
30% glycerine-H_2O solution	1.075	22.32×10^{-4}	7.11×10^{-2}	0.02
Freon 12	1.315	3.53×10^{-4}	0.90×10^{-2}	5.78
Freon 21	1.35	3.60×10^{-4}	0.69×10^{-2}	1.56

[a] for $T = 21°C$.

Table 3 Wavelength and amplitude progression along jet windward surface, $d_j = 0.079$ cm

$\bar{q}$	18.6		13.2		12.7		11.0		10.8		10.1		6.68		4.33	
M	2.4		2.4		2.4		4.0		2.4		2.4		2.4		2.4	
Liquid	H_2O		H_2O		glyc-H_2O		H_2O		CS_2		H_2O		H_2O		H_2O	
Starting pt., y, cm	0.201		0.173		0.198		0.198		0.104		0.158		0.165		0.117	
	λ/d_j	a/d_j	λ/d_j	a/d_j	λ/d_j	a/d_j	λ/d_j	a/d_j	λ/d_j	a/d_j	λ/d_j	a/d_j	λ/d_j	a/d_j	λ/d_j	a/d
	0.29	0.10	0.48	0.29	0.38	0.10	0.70	0.45	0.45	0.22	0.74	0.008	1.22	0.35	0.29	0.13
	0.029	0.10	0.58	0.29	0.48	0.26	0.61	0.51	0.58	0.16	0.99	0.51	0.38	0.29	0.51	0.16
	0.29	0.22	0.74	0.29	0.48	0.38	0.54	0.22	0.45	0.22	1.50	0.51(m)	1.25	0.58(s)	0.93	0.19
	0.45	0.15	0.58	0.71	0.54	0.29	0.54	0.29	0.58	0.16	0.80	−(s)	1.34	0.48	1.06	0.45
	0.48	0.19	0.96	0.48	0.58	0.35	0.77	0.51	0.51	0.16	0.99	0.35	2.24	0.29	1.22	0.41
	0.38	0.29	1.38	0.48	0.54	0.26	2.27	0.77(m,s)	1.02	0.35	1.98	0.54(f)			1.70	0.26
	0.48	0.35	0.67	0.19(s)	1.12	0.54(s)	2.50	0.93	2.14	0.74(s)					1.47	0.26
	0.29	0.05	1.22	0.48(s)	1.12	0.77	1.66	0.29	0.86	0.58						
	0.35	0.29	1.44	0.22	1.22	0.77	1.66	−(f,c)	1.02	0.58						
	0.15	0.05	1.44	0.22(m)	1.44	0.45	2.21	−(c)								
	0.74	0.38	1.22	1.95(f,c)												
	0.96	0.45	1.44	1.95(c)												
	0.38	0.15														
	0.67	0.48														
	0.64	0.58														
	0.77	0.16(s)														
	0.67	0.35(s)														
	0.74	0.58														
	2.43	0.067(f)														

Notation: s = sonic point location on shock, f = jet fracture location, m = multicrested wave, c = wave visible in detached clump.

Table 4 Wavelength and amplitude progression along jet windward surface, $d_j = 0.159$ cm

$\bar{q}$	6.47		4.88		5.12		3.66		3.58		2.63		1.91	
M	2.4		2.4		4.0		2.4		2.4		2.4		4.0	
Liquid	H_2O		H_2O		H_2O		CS_2		H_2O		H_2O		H_2O	
Starting pt., y, cm	0.173		0.231		0.061		0.180		0.150		0.178		0.081	
	λ/d_j	a/d_j	λ/d_j	a/d_j	λ/d_j	a/d_j	λ/d_j	a/d_j	λ/d_j	a/d_j	λ/d_j	a/d_j	λ/d_j	a/d_j
	0.48	0.19	0.85	0.24	0.98	0.51	0.59	0.26	0.59	0.19	0.80	0.48	0.26	0.10
	0.48	0.22	0.48	0.10	0.35	0.10	0.96	0.26	0.75	0.37(s)	0.85	0.12	0.99	0.26
	0.56	0.24	0.96	0.29(s)	0.90	0.98	2.00	0.59(m)	1.04	0.26	0.72	0.34(s)	1.02	0.38(s)
	0.85	0.34(m)	0.96	0.43	1.02	0.51(s)	1.60	0.38(s)	1.25	0.50(m)	0.72	0.14	0.82	0.08
	0.37	0.10	0.96	0.43	0.77	0.22			1.49	0.70(m,f)	0.72	0.14	1.07	0.26(f)
	0.38	0.19	1.26	0.37(f)	0.77	0.26					4.96	0.14		
	0.61	0.18(s)			0.90	0.21					0.85	0.14(f)		
	0.72	0.19			0.90	0.21								
	9.3	0.22			1.54	0.61(f,c)								
	1.20	0.34												

Notation: s = sonic point location on shock, f = jet fracture location, m = multicrested wave, c = wave visible in detached clump.

the jet for a given injector size, independent of $\bar{q}(\equiv \rho_j V_j^2/\rho_\infty V_\infty^2)$. This location is about $y/d_j = 2$ for the 0.079 cm jet and $y/d_j = 1.5$ for the 0.159 cm jet and is approximately where the jet begins to curve downstream. The absolute value of the wavelengths and amplitudes are generally slightly greater in this region for the 0.079 cm jet than for the 0.159 cm jet.

The second group of waves has longer wavelengths, ranging about $\lambda/d_j \approx 0.5$-0.8. These waves often appear to be sets of two or three of the earlier waves bunched into one. The amplitudes are greater than the earlier waves and increase with arc length along the jet. There is usually little space between the convex portions of the waveform. That is, the waves are approximately square with the trough length considerably shorter than that of the crests. The jet has not curved significantly at the onset of this group of waves, and it continues to curve only gradually throughout most of the length of their presence. There are always at least two of these "intermediate" waves, usually more, the number depending on $\bar{q}$. The wave sizes are comparable for both size jets.

The second group of waves ends at the sonic point behind the bow shock in the plane of the jet trajectory. The usual effects are immediate flattening and lengthening and elimination of surface irregularities. Often the sonic point is adjacent to a sharp wave crest, where a steep wave has risen and then smooths out and lengthens. Just beyond the sonic point is usually a transition region, particularly noticeable when the shock remains near the sonic angle for some distance, where a shorter, steep wave (or waves) may appear. The principal trend is to long, flat waves which continue until fracture, and these form the third group of waves. It is important to note that the absolute amplitudes of these "flat" waves are greater than the earlier waves, but because of their long wavelength and absence of sharp crests, they appear relatively flat.

Near the sonic point location, the jet body has curved some 25-30 deg from the initial vertical, but curvature to that point has been gradual and the derivative of the trajectory fairly constant. In the transition region, however, the curvature often increases, and the slope decreases rather rapidly for a distance and then becomes nearly constant again until fracture. The long waves in this third region are usually from $\lambda/d_j \approx 1.0$-1.5 in wavelength. The amplitude usually ranges from one-half to one-third of λ, with some gradual steepening along the jet to fracture. Often waves of this type are visible in recently detached clumps. The clumps are usually 2-4 λ long, and there is usually a noticeable step at the point of detachment.

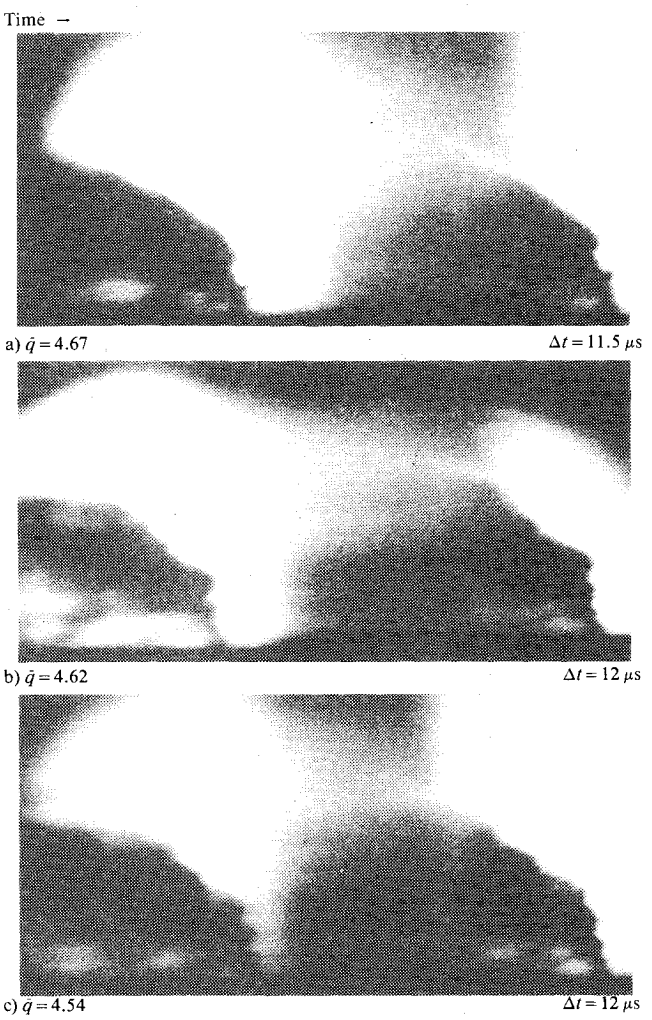

Fig. 3 Rotating mirror camera sequences, $d_j=0.159$ cm, H_2O, $M=2.4$.

Finally, it is important to note that the data show that the wave process is not a strong function of injectant physical properties as can be seen by comparing the results for water with those for Freon, carbon disulfide, and glycerine-H_2O solutions. This finding has very important implications with regard to theoretical modelling.

Wave Speed Measurements

The two-picture sequences obtained with the rotating mirror camera show the instantaneous jet configurations at an interval of a few microseconds; a typical result is shown in Fig. 3. Specific wave crests or troughs on the windward surface were identified in each picture, and their movement along the local direction of the jet axis during the known time interval was measured. Dividing the axial displacement by the time increment gave an average local axial wave velocity. This velocity consists of the local liquid velocity, which convects the disturbance along the jet, and an axial wave propagation velocity, if any, relative to the liquid.

The velocities determined, designated by V_w, have been plotted versus arc distance along the jet windward surface during the measuring interval. The results are shown in Fig. 4. The data points are classified by $\bar{q}$ level, and the corresponding V_j for each $\bar{q}$ is given. As can be seen, there is considerable scatter, which is not surprising due to the process' unsteadiness and measurement difficulty, but there is a clear trend of increasing velocity along the jet. There is no clear segregation of points with $\bar{q}$ for either jet size.

From Fig. 4, it can be seen that the velocities on the larger jet are higher than those for the smaller jet. This result seems

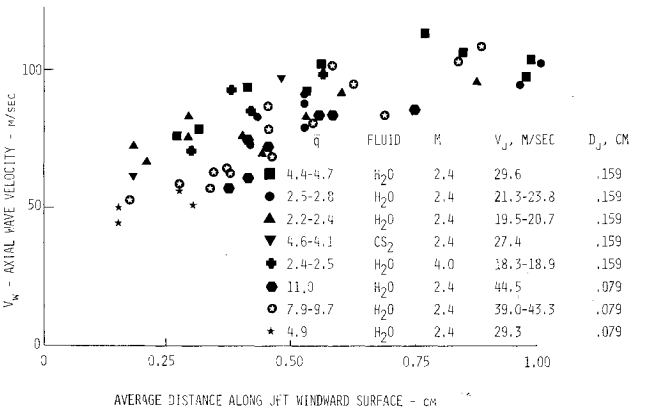

Fig. 4 Measured axial wave velocities.

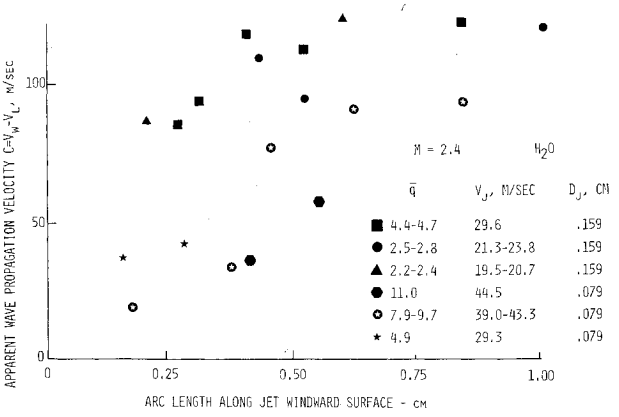

Fig. 5 Deduced wave propagation velocities.

surprising; V_j for the 0.079 cm jets was higher (30-50 m/s) than for the 0.159 cm jet (20-30 m/s). The existence of downstream running waves, greater in wave speed on the larger jet than the smaller jet, could cause the results for V_w obtained. In the general case, traveling waves propagate in opposite directions from the disturbance origin. There is theoretical work that indicates that upstream-running waves in this type of gas-liquid system are damped out rapidly.

There is considerable evidence in the data to suggest the presence of axial wave propagation. Even early in the jet trajectory, where little curvature and acceleration has occurred, the measured velocities are substantially higher than the jet bulk exit velocities. The situation can be investigated further by the use of spark microphotos. From the spark photos, the jet trajectories can be clearly observed, and the amount the jet axis has turned from the vertical at the location of a disturbance used for measurement in the rotating mirror camera sequence can be measured. This local curvature is determined by the downstream velocity V_x relative to the normal component V_y. The local liquid velocity V_L will have orthogonal components V_x and V_y. In order to estimate the local liquid velocity in the jet, we have made some simplifying assumptions. By assuming conservation of normal momentum and a negligible change in jet cross-section area, we can take $V_y=V_j$. Dividing this value by $\cos\theta$, where θ is the angle the jet has turned from the vertical, yields the magnitude of the local liquid velocity. The results are plotted in Fig. 5 in terms of (V_w-V_L). They show that there is a definite wave propagation velocity, $c\equiv V_w-V_L$, and that it increases with arc length.

High-Speed Motion Picture Observations

No matter how many still pictures of various types are observed, it is impossible to fully appreciate the true, unsteady nature of the jet phenomena without viewing high-speed movies of the injection process. One sees a number of

cyclical motions occurring simultaneously with different high frequencies. These include the movement of waveforms along the jet, the fracture of clumps of varied sizes and shapes at different locations along the outer portion of the jet, the clump breakup after detachment, the oscillation of the jet body—including a "snapping" effect in the outer portion as the clumps fracture, oscillation of a liquid layer on the plate, and various unsteady gross movements of the entire jet. Also, certain distinct types of clumps seem to appear periodically as do large waves along the jet.

The gross movements of the jet clearly have major significance in the overall jet behavior, and a further description and classification of them is warranted. For low $\bar{q}$ cases, there is a continuous vibration and whipping motion of the entire jet. These motions, either entirely or in part, could be related directly to the clump detachment process. There are apparently at least two distinct motions superimposed, one corresponding to continuous oscillation of the jet column and one related to clump detachment. In fact, the whipping of the jet could be a determining or contributing factor in the causing the clumps to detach. The high $\bar{q}$ case behavior can be described as characterized by a relatively steady main jet body. There is a substantial movement of the outer region of the jet, however, in that portion which eventually becomes a clump. There are not the overall undulations and large amplitude whipping that occurs for lower $\bar{q}$, but there is a noticeable "snap" of the outer jet, including upstream movement, as clumps detach. It is difficult to tell whether the jet snaps with every clump or only with certain large ones or if the amount of motion is a matter of degree related to clump size. It is an interesting and important question to consider whether the fracture is caused primarily or in part by the unsteady motion of the jet "throwing off" clumps when they become a critical size.

The purpose of the movies was to attempt to quantify the various events in the jet, as well as to obtain a qualitative picture of the dynamics. The quantitative study turned out to be an extremely difficult task. It was difficult to count the frequency of the waves moving along the jet. The best means of deriving quantitative information from the movies was by stop action. A single frame projected onto the screen shows four pictures at once because of the quarter-frame method of photography, and the film can be advanced manually a picture at a time. These still pictures are at intervals of 1/36,000 s or about 28 μs. It was found that for 0.079 cm jet, high $\bar{q}$ tests, a clump was fractured approximately every second frame, or a frequency of 18,000 s^{-1}. The best movies of the 0.159 cm jet in which clump fracture could be observed were at $\bar{q} = 1.2$. A count of the clump break-offs from a stop-action survey gave an average over many frames of 12,000 clumps/s, but there were intervals where the rate was as high as 14,000 clumps/s and other as low as 9400 clumps/s.

Discussion

Experimental studies aimed at quantification of some of the details of transverse liquid jet breakup were concluded. The principal results may be summarized as follows. First, the breakup process is a result of large amplitude surface waves that form on the jet column. The waves surround the jet column. Perhaps surprisingly, it was found that the formation and behavior of these waves is insensitive to rather large variations in surface tension and viscosity. It was possible to classify the surface waves into three groups depending upon location along the jet trajectory and relative to the sonic point behind the interaction shock. Second, the surface waves on the jet column were shown to propagate in the downsteam direction at a sizeable velocity of the order of the injection velocity. Third, the behavior of the jet as a whole is composed of several, superimposed cyclical motions with different, but all high (order 10^4 s^{-1}), frequencies. The behavior at low $\bar{q}$, where the whole jet oscillates violently, is different from that at high $\bar{q}$, where the initial portion of the jet column is rather steady. It is also interesting to note that the studies reported in Ref. 5 showed that quite different, very sharp, wave forms occur for downstream angled injection.

The results presented here can be used as the basis for some conjectures as to the causes of the waves on the liquid column that lead to breakup. Broadly speaking, these waves could be either surface tension waves, gravity (or "acceleration") waves, Kelvin-Helmholz waves, or eddies due to turbulence. This last possibility is suggested by the peculiar resemblance between high-speed movies of the type discussed here and smokestack plumes in a crosswind. The fact that the waves observed on the liquid column have a substantial propagation velocity would, however, seem to rule out the "turbulence" model. The surface tension wave breakup mechanism of liquid jets in the absence of a cross flow made famous by Rayleigh also can apparently be ruled out, since the effect of variations in surface tension of the injectants was negligible. The acceleration sensed by the curved, windward jet surface is quite large and can certainly be expected to support the creation of surface waves. The liquid surface on the leeward side of the jet could also have waves by the same mechanism. However, the side surfaces of the jet column do not have an acceleration vector in the correct direction to produce surface waves. Waves were observed on the side surfaces, but these could be simply the passive result of nearby waves formed on the windward and leeward sides. Further evidence in support of the acceleration wave mechanism is found in the fact that the waves begin to appear and grow only where the jet column has begun to curve. For the Kelvin-Helmholz mechanism, one needs relative flow. There is clearly a large difference in the axial gas flow over the windward side of the jet after the column has curved over and the liquid flow in the jet. The same cannot, however, be said for the leeward side of the jet, and waves were seen to form there also. Summing up, the present results seem to point to the acceleration wave mechanism as the most likely cause of transverse liquid jet breakup.

Acknowledgment

This work was supported by the Air Force Office of Scientific Research. Technical monitoring was by Dr. B. T. Wolfson.

References

[1] Sherman, A. and Schetz, J. A., "Breakup of Liquid Sheets and Jets in a Supersonic Gas Stream," *AIAA Journal*, Vol. 9, April 1971, pp. 666-673.

[2] Kush, E. A., Jr., and Schetz, J. A., "Decomposition of a Liquid Jet Injected Normal to a Supersonic Air Stream," AFOSR TR-72-1180, June 1972.

[3] Joshi, P., Jakubowski, A. K., and Schetz, J. A., "Effect of Injector Geometry on Penetration, Spread and Structure of a Liquid Jet Injected Normal to a Supersonic Air Stream," AFOSR-TR-74-0149, Sept. 1973.

[4] Schetz, J. A., Kush, E. A., Jr., and Van Overeem, J., "High-Speed Photographic Study of Liquid Jet Break-up in a Supersonic Airstream," Ninth International Congress on High Speed Photography, Denver, Colo., Aug. 1970.

[5] Baranovsky, S. I. and Schetz, J. A., "Effect of Injection Angle on Liquid Injection," AIAA Paper 79-0382, Jan. 1979.